



LAWRENCE
LIVERMORE
NATIONAL
LABORATORY

Evaluating a Simple Fracturing Criterion for Hydraulic Fracture Crossing Stress and Stiffness Contrasts

J. Huang, P. Fu, R. R. Settgast, J. P. Morris, F. J.
Ryerson

May 21, 2018

rock mechanics and rock engineering

Disclaimer

This document was prepared as an account of work sponsored by an agency of the United States government. Neither the United States government nor Lawrence Livermore National Security, LLC, nor any of their employees makes any warranty, expressed or implied, or assumes any legal liability or responsibility for the accuracy, completeness, or usefulness of any information, apparatus, product, or process disclosed, or represents that its use would not infringe privately owned rights. Reference herein to any specific commercial product, process, or service by trade name, trademark, manufacturer, or otherwise does not necessarily constitute or imply its endorsement, recommendation, or favoring by the United States government or Lawrence Livermore National Security, LLC. The views and opinions of authors expressed herein do not necessarily state or reflect those of the United States government or Lawrence Livermore National Security, LLC, and shall not be used for advertising or product endorsement purposes.

Evaluating a Simple Fracturing Criterion for a Hydraulic Fracture Crossing Stress and Stiffness Contrasts

Jixiang Huang, Pengcheng Fu*, Randolph R. Settgast, Joseph P. Morris and Frederick J. Ryerson

Atmospheric, Earth, and Energy Division, Lawrence Livermore National Laboratory, Livermore, CA 94550, U.S.A.

*Corresponding author: fu4@llnl.gov, +19254223579

Abstract

Hydraulic fracture height containment is a critical issue in the development of unconventional reservoirs. The extent of fracture height growth depends on a variety of factors, particularly stress and stiffness contrasts between adjacent layers. Accurate simulation of fracture growth and containment requires a reliable fracturing criterion. The virtual crack closure technique (VCCT) is a widely used method for computing energy release rate. However, it is based on the assumption that a small crack extension does not significantly alter the state of the crack tip, which is generally not the case when a fracture crosses strong stress and/or stiffness contrasts. In this work, we assess the applicability and accuracy of a modified virtual crack closure technique (MVCCT) for a fluid-driven fracture in breaking through interfaces with significant stress and/or stiffness contrasts, through comparisons with analytical and reference numerical solutions. The results show that significant error could occur when the fracture tip is very near or at stress/stiffness interfaces. However, this error is localized to the interface and proves to be inconsequential to the predicted penetration depth into the rock layer beyond the interface. This study validates the applicability of MVCCT in 3D hydraulic fracturing simulation in strongly heterogeneous rock formations.

Keywords: hydraulic fracture · fracturing criterion · VCCT · stress contrast · stiffness contrast

List of symbols:

E	Young's modulus
G	Energy release rate
G_c	Critical energy release rate
G_I	Energy release rate for Mode I
K_{Ic}	Critical stress intensity factor for Mode I (known as "fracture toughness")
U	Elastic strain energy
W	Potential energy of the applied loading
Π	Total potential energy
$\boldsymbol{\varepsilon}$	Strain tensor
\mathbf{C}	Stiffness matrix
\mathbf{b}	Body force
\mathbf{f}	Nodal force

h	Half fracture height
h_0	Half thickness of middle-layer or the layer that the fracture is propagating from
p	Fracture pressure
$\hat{\mathbf{t}}$	Boundary force
ν	Poisson's ratio
w	Fracture width
σ	<i>In situ</i> stress magnitude
$\Delta\sigma$	Stress contrast magnitude

1 Introduction

Vertically oriented hydraulically driven fractures are generally created within hydrocarbon reservoirs where the minimum principal stress is typically in the horizontal plane. Height growth of vertical hydraulic fractures is of particular interest for both economic and environmental considerations. From an economic perspective, contained fracture height growth can be either beneficial or problematic depending on the circumstances. If the target pay zone is thin, vertical containment with sufficient lateral fracture extension is favored to minimize the waste of fracturing material and energy in nonproductive formations, as well as the water production from non-hydrocarbon formations. On the other hand, in thick reservoirs consisting of multiple production zones, height containment may make stimulating the entire reservoir depth interval difficult, which ultimately may necessitate multiple horizontal laterals at different depths to produce the entire target interval. From an environmental perspective, secured containment is much favored to prevent the creation of potential communication pathways for fracturing fluids or hydrocarbons to pollute shallow aquifers (Maxwell 2011).

As one of the most critical and challenging issues in hydraulic fracturing, the mechanisms and predictions of fracture height containment have been the subject of numerous studies. For a fracture vertically spanning a rock formation and under pressure that sustains its lateral growth, whether the fracture can propagate into or to what extent it can propagate into an adjacent formation depends on a number of factors: differences in *in situ* states or properties (elastic properties, fracture toughnesses, and permeabilities) between the two formations, ductility of the rocks, the presence of natural fractures, the properties/states of the horizontal interface between the two formations, and relative formation thickness in the vicinity of the fracture, to name a few. Among these factors, the *in situ* stress contrast between adjoining layers has been recognized as the principal mechanism that contains fractures in most scenarios, especially at great depths

(Mader 1989; Fisher and Warpinski 2012). Following the early work by Perkins and Kern (1961), extensive numerical, laboratory and mineback studies have been performed to understand the importance of stress contrast (Simonson et al. 1978; Warpinski et al. 1982a; Voegele et al. 1983; Palmer and Luiskutty 1985). In rock formations, *in situ* stress variation is often induced by variation of rock properties, particularly elastic properties, so the effects of a stress contrast must be considered together with formation stiffness and layer thickness. Stiffness contrast, however, by itself has been found to have limited effect on fracture height growth and concluded not to be a significant containment mechanism (Fung et al. 1987; Smith et al. 2001). Both theoretical and experimental studies have also demonstrated that fracture toughness varies over a rather narrow range and is thus not usually treated as a variable in assessing fracture height growth (Hanson and Shaffer 1980; van Eekelen 1982; Warpinski et al. 1982b; Teufel and Clark 1984; Hsiao and El Rabaa 1987). In addition, the measured values of toughness already embody many local effects (e.g., ductility) around the fracture tip, which decrease stress intensity factor or increase effective fracture toughness, as suggested by van Eekelen (1982). However, there are some factors that may also play a role in fracture containment when the stress contrast is not the predominant factor. For example, interface slippage, expected to occur at shallow depths, has the potential to fully terminate fracture height growth, activate interface fractures, or cause offsets in the fracture (Lam and Cleary 1984). Therefore, a perfect bonding assumption between formation layers is appropriate only under certain conditions, which have been well studied analytically (Lam and Cleary, 1984), experimentally (Daneshy, 1978; Teufel and Clark, 1984), and numerically (Cooke and Underwood, 2001; Zhang and Jeffrey, 2008).

Fracture containment in complex geological settings has been evaluated by a variety of recently developed numerical models (Sheibani and Olson 2013; Abbas et al. 2014; Chen et al. 2015; Chuprakov and Prioul 2015; Zhou et al. 2016; Li, et al. 2016; Zhou et al. 2017; Zhang et al. 2017; Huang et al. 2018). In a numerical model, a fracturing criterion determines when and along which direction a fracture should propagate from the current fracture front. According to the equilibrium law in fracture mechanics, a fracture propagates if the stress intensity factor (SIF), or interchangeably energy release rate, exceeds a critical value, which is an intrinsic property of the host rock. There are various methods to calculate SIF in the context of the finite element method (FEM) or boundary element method (BEM), including direct methods through stress or displacement extrapolation and energy-based indirect methods such as the *J*-integral, the stiffness

derivative technique, and virtual crack extension (Cherepanov 1967; Rice 1968; Parks 1974; Rybicki and Kanninen 1977). The direct methods rely on accurate field representations around the crack tips which generally require a very fine mesh, special crack tip elements, or a correction factor (Tracey 1971; Fu et al. 2012). The energy-based indirect methods have been widely used and demonstrated to be reasonably accurate on relatively coarse meshes (Li et al. 1985).

One of the energy-based indirect methods, the virtual crack closure technique (VCCT), originally proposed by Rybicki and Kanninen (1977) based on Irwin's crack closure integral and later extended by other researchers (Shivakumar et al. 1988; Krueger 2004), is recognized as an efficient and practical method in many aspects. In the three-dimensional space, it avoids many difficulties associated with other methods, such as requiring singularity elements at the crack front and creating elements normal to the curved crack front (Leski 2007), and the difficulty in separating SIF components in mixed-mode fracture problems. Another advantage is that it is amenable to the implementation in parallel computing because the calculation in VCCT relies only on the states of elements directly connected to the tip so the communication between processors is minimized in distributed memory computing environments (Settgast et al. 2017). However, a fundamental assumption behind VCCT might make its application in the evaluation of fracturing near stress/stiffness contrast problematic. The formulation of VCCT assumes a finite virtual crack extension (typically by one single element length) does not significantly alter the state of the crack tip so that the separation near the virtually extended fracture can be approximated by the displacements behind the crack tip in the current configuration. This assumption makes it possible to evaluate the energy release rate in the current configuration without having to actually create the virtual extension. The self-similarity assumption, however, limits the utilization of traditional VCCT in non-planar cracks (Xie and Biggers 2006), and may also become problematic when a crack crosses strong stress or stiffness contrast, which is inherently the case for fracture containment mechanisms.

Many methods have been well established to model hydraulic fracture growth in largely homogeneous rocks (e.g., Barree 1983; Clifton and wang 1988; Weng et al 2011; McClure and Horne 2013; Wu and Olson 2015). Although stiffness and stress variations can lead to significant complication in fracture modeling, most existing models use an upscaled effective value to smear out the stiffness variation for simplicity and computational efficiency. The applicability of these

existing methods under such conditions has not yet been adequately addressed. To this end, the objective of the current study is to evaluate the applicability and accuracy of VCCT, more specifically, a modified version (MVCCT) for fluid-driven fracturing, at and near the interface between two adjoining rock layers with significant *in situ* stress and/or stiffness contrasts. We consider the most typical fracturing scenario where the hydraulic fracture primarily extends horizontally whereas vertical fracturing across the interface and into the next layer determines the height of the fracture. The structure of the present paper is as follows. First, we introduce the fracture mechanics framework in section 2 within which the study is undertaken. Then, we briefly review the formulation of MVCCT in section 3. Section 4 presents the formulation of a direct energy difference method (DEDM), which calculates the fracture tip energy release rate via its very definition. Although impractical, this method will be used to provide the “ground truth” solution for energy release rate when an analytical solution is unavailable. In section 5, we study the accuracy of MVCCT near the stress contrast by comparing its solutions to corresponding closed-form solutions and DEDM results. This comparison also verifies our particular implementation of DEDM. We finally study the effectiveness of MVCCT near the rock stiffness contrast, including when stress and stiffness contrasts coexist.

2 Fracture Mechanics Framework

The current work is built within the following fracture mechanics framework:

- We use linear elastic fracture mechanics (LEFM) and an energy-based fracturing criterion. The criterion states that a fracture extends if the energy release rate of the system corresponding to the said extension is greater than the critical energy release rate G_c of the material that the fracture tip is propagating in or into. Note that energy release rate is a state variable of the entire system concerned in the analysis and this system could be homogeneous or heterogeneous. The critical energy release rate is a property of the materials that the fracture is propagating in or into.
- The critical stress intensity factor K_c , introduced by Irwin (1948), also known as fracture toughness, can be derived from G_c . For mode-I fracturing, the only mode concerned in this work, the relationship

$$G_c = K_{Ic}^2 \left(\frac{1 - \nu^2}{E} \right) \quad (1)$$

where E is Young's modulus and ν is Poisson's ratio.

- In the context of LEFM, it is common to use $K_I \geq K_{Ic}$ as the criterion to determine when the fracture extends. Here K_I is a state variable and K_{Ic} is a material property. However, the concept of SIF is a theoretical construct usually applied to a homogeneous, linear elastic material, defined as the factor that correlates the stress near the crack tip with the square root of polar coordinate r . Strictly speaking, when the tip is near the bi-material interface, the power of singularity is no longer $-1/2$ and therefore such a factor does not apply. However, a common practice is to adapt this factor by introducing a correction factor. To avoid this theoretically cumbersome treatment, we use the energy-based criterion $G_I \geq G_c$, which can be directly evaluated with MVCCT or similar methods.
- Our analysis does not require the involvement of K_I or K_{Ic} , but they are still used when investigating fracturing near a stress contrast in a homogeneous formation to make the narrative conforming to a more conventional framework. In Section 5.2, when we investigate the effects of spatially varying stiffness, one of the scenarios considered is that the rock layers have the same K_{Ic} , which is rooted in a common observation from laboratory fracture toughness testing (van Eckelen 1982; Thiercelin et al. 1989). However, K_{Ic} here is only an intermediate concept to derive G_c for individual materials and K_{Ic} itself is not used in our analyses.

3 Modified Virtual Crack Closure Technique

The original VCCT formulation assumes zero traction on the fracture surface. Considering that hydraulic fracturing is driven by high fluid pressure exerted on the fracture surface, a modified virtual crack closure technique (MVCCT) is required to calculate the energy release rate and SIF under this condition (Raju 1987; Settghost et al. 2017). We briefly review the formulation of MVCCT to provide a proper context for the subsequent analyses.

Fig. 1 shows a mesh configuration for Mode-I calculation. Here a 2D projection of a 3D geometry is shown to illustrate the concepts: an edge (the fracture front) in 3D collapses into a node in 2D while a face in 3D collapses into an edge in 2D. In MVCCT, the quantities for calculating the SIF are only required on one side of the fracture plane due to symmetry, while the elements on the opposite side of the fracture plane are shown in gray lines in the figure. Like the original VCCT, MVCCT assumes that the energy released when the crack is virtually extended for a certain distance is identical to the energy required to close that crack. Furthermore, it assumes that a small crack extension does not significantly alter the state at the crack tip. That is to say, when the crack tip is located at *node a*, the displacement (i.e., half fracture opening $w_b/2$) and the external force due to fluid pressure $f_{external}^b$ on the surface behind the crack tip at *node b* (referred to as the “trailing node” hereafter) are approximately equal to the those at *node a* with crack tip at *node a'*. Under this self-similarity assumption, forces and displacements required to calculate the energy to close the crack can be obtained from a single finite element analysis (as opposed to computing two states, with and without the virtual growth, separately). Specifically, the energy release rate G for splitting *node a* (or the corresponding element edge in 3D) is approximated by the work done by the closure forces moving a distance divided by the newly generated surface area A ,

$$G_I = -\frac{1}{2A}(f_{disconnected} - f_{external}^b) \cdot w_b \quad (2)$$

where $f_{disconnected}$ is the force on *node a* normal to the fracture plane resulting from the volume integral on the divergence of the stress tensor from the finite elements on one side of the fracture plane, and $f_{external}^b$ is the nodal force on *node b* normal to the fracture plane resulting from any externally applied loads (e.g. fluid pressure). Note that the force $f_{disconnected}$ involves the volume integral on the elements that are both behind (e.g., element I for *node a*) and ahead (e.g., element II for *node a*) of the fracture tip. When the tip is at the interface of stress or stiffness contrast, the resulting force and opening at the tip node could be significantly different from those when the tip has passed the interface (say, at *node a'*), violating the self-similarity assumption.

4 Direct Energy Difference Method for Ground Truth Value

Although a comprehensive set of analytical solutions for SIF in different fracture configurations are available in the literature (e.g., Tada et al. 2000), we utilize numerical methods for the scenarios considered in the current study for which analytical solutions are not available. We use a direct energy difference method (DEDM) based on a direct computation of the system potential energy release as the ground truth. The MVCCT will be validated against the available analytical solutions, as well as DEDM when an analytical solution is not available.

For a crack in an elastic body subject to a load, the energy release rate is defined as the decrease in the total potential energy of the system when the crack is extended by a unit area. The total potential energy Π includes both elastic strain energy and the potential energy of the applied loading (as if the loading is caused by a conservative force), given by

$$\Pi = U - W \quad (3)$$

where U is the strain energy stored in an elastic material undergoing deformation that can be expressed in terms of the strain $\boldsymbol{\varepsilon}$ and stiffness matrix \mathbf{C}

$$U = \frac{1}{2} \int_{\Omega} \boldsymbol{\varepsilon}^T \mathbf{C} \boldsymbol{\varepsilon} d\Omega \quad (4)$$

and W is the potential energy of the applied loading that is the sum of contributions from the given interior (body) force \mathbf{b} and exterior (boundary) force $\hat{\mathbf{t}}$

$$W = \int_{\Omega} \mathbf{u}^T \mathbf{b} d\Omega + \int_{\Gamma_t} \mathbf{u}^T \hat{\mathbf{t}} d\Gamma_t \quad (5)$$

where \mathbf{u} is the displacement. The boundary integral, that is, the second term in Eq. (5), is taken only over the portion of the boundary Γ_t where tractions or forces are specified.

In our implementation of DEDM, the states of the body containing a crack are determined by the finite element method so that the potential energy stored in the body can be obtained by integrating over all elements in the reference configuration. A second configuration is then created by extending the crack slightly (typically, by one element size) and an updated potential energy in the body is computed. The ratio between the difference in the potential energy and the difference in the crack area is, by definition, the energy release rate. This procedure is rarely directly used in

solving boundary-value problems because of its low computational efficiency. However, it does produce consistent and reliable solutions, and therefore is used to provide a meaningful benchmark case. It bears noting that a numerical precision problem arises when the magnitudes of potential energies in the two configurations are large numbers compared with the difference between them. In some cases, the available numerical precision is insufficient to provide accurate results. To mitigate this problem, rather than calculating the difference between the summations of element energy, we compute energy differences between the two states for all individual elements and sum the differences. In addition, a large computational domain (tens of fracture lengths in each dimension) with graded mesh is used to minimize the boundary effects. We have verified the accuracy of DEDM on numerous configurations and boundary conditions included in Tada et al. (2000), of which most are for semi-infinite cracks embedded in isotropic homogeneous media. The relative error is well below 1% if proper tip-region mesh resolutions are adopted. We also validated DEDM against the analytical solution for a finite fracture approaching a perpendicularly-oriented, bi-material interface (Cook and Erdogan 1972), where DEDM shows reasonable accuracy even under extreme modulus contrasts. The detailed comparisons are not shown here, but the comparison with the analytical solution for the equilibrium height model in the next section can serve as a direct verification for DEDM. Note that the methodology of DEDM, formulated according to the definition of energy release rate, requires no underlying assumption of homogeneous media. The accuracy of DEDM is only limited by the FEM formulation's ability to quantify elastic potential energy under the given materials, fracture, boundary condition, and mesh resolution configurations.

5 Numerical Results

In this section, we investigate scenarios where a fracture is approaching and subsequently crossing the interface between two rock layers with distinct stresses and/or stiffness contrasts. We assume the fracture to be perpendicular to the bedding plane, implying horizontal bedding and a vertical fracture, the most typical scenario for unconventional oil and gas development. The bedding planes are assumed to have perfect bonding (i.e. no slippage). We also assume pseudo-static plane-strain condition for the following considerations. First, in a fracture primarily experiencing lateral growth, fluid flow along the vertical direction and thereby the viscous loss within a vertical cross-section that we consider herein is minimal. Second, even if the overall fracturing is in the viscosity-

dominated regime, the height growth in each vertical cross-section is determined by the fracture's ability to overcome stress/stiffness/toughness barriers in the corresponding plane-strain setting. In fact, the plane-strain condition and zero-pressure gradient within each vertical cross section have been common assumptions for most analytical solutions for hydraulic fracturing (Adachi et al. 2010; Liu and Valko 2017).

5.1 Fracturing near a stress contrast

A classic equilibrium-fracture-height model, i.e., a vertical fracture under the plane-strain condition subjected to uniform internal pressure and vertically-varying horizontal *in situ* stresses, is used to assess the applicability of MVCCT when the fracture is approaching and crossing a stress contrast. The conceptual model is illustrated in Fig. 2, where the fracture vertically spans three horizontal layers. The hydraulic fracture originates from the middle layer in the analysis and our focus is on the fracture's propagation into the upper and lower formations under high confining stress.

The stress contrast $\Delta\sigma$ between the middle layer and the upper layer and that between the middle and lower layers are the same, establishing symmetry against the mid-height horizontal plane. The analytical solution of the SIF at each tip of the fracture, when the fracture extends by a length x into the upper and lower layers, is given by Simonson (1978) as

$$K_I = (p - \sigma_h - \Delta\sigma)\sqrt{\pi h} + 2\Delta\sigma \sqrt{\frac{h}{\pi}} \sin^{-1}\left(\frac{h_0}{h}\right) \quad (6)$$

where p is the fluid pressure in the fracture, σ_h and h_0 are the confining stress and half-thickness in the middle layer, $\Delta\sigma$ is the stress difference between the high-stress layer and low-stress layer, h is the total half height of the fracture, and K_I is the stress intensity factor at the tips.

In our validation case, the middle layer thickness is set to $2h_0 = 20$ m, and stress difference at the interfaces $\Delta\sigma = 2$ MPa. Fracture toughness has been shown to vary within a small range in laboratory experiments (e.g., Hsiao and El Rabaa 1987) and is therefore not considered a salient variable for the current analysis. The potential scale dependence of fracture toughness is not yet well understood and may constrain fracture growth in a way that is beyond the scope of current investigation (Delaney et al. 1986; Shlyapobersky et al. 1998; Scholz 2010). For the purpose of

this paper, the formation toughness is assumed $K_{Ic} = 1 \text{ MPa}\cdot\text{m}^{1/2}$ (i.e., $G_c = 93.75 \text{ J/m}^2$). For a half-height $h_0 = 10 \text{ m}$, we start the investigation with a mesh resolution $\Delta h = 0.25 \text{ m}$ along fracture growth direction. The summary of specific material and geometry parameters is listed in Table 1. Results from MVCCT and DEDM are both validated against the analytical solution. Since neither method directly calculates the propagation depth nor the fracture length, an iterative procedure is used to derive the equilibrium fluid pressure (referred to as the “fracturing pressure” hereafter) that yields $G_I = G_c$ (interchangeably $K_I = K_{Ic}$ under homogeneous condition) for the given fracture length.

Fig. 3 compares the predictions of fracturing pressure from the three methods (analytical, MVCCT, and DEDM), namely the pressure required to propagate the fracture from the current length as a function of the penetration depth x from the interface into the higher-stress layer. We express the results in terms of net fracturing pressure $\Delta p = p - \sigma_h$, defined as the difference between the fracturing pressure and the minimum horizontal stress at the layer where fracture initiates (i.e., the middle layer in Fig. 2), to eliminate σ_h as a variable. The net fracturing pressure decreases monotonically with fracture extension before it reaches the stress barrier but drastically increases once it penetrates into the stress barrier, where the rate of increase then becomes rather modest after a certain penetration. It is worth noting that stress barriers (and also stiffness barriers in next subsection) do not inhibit a fracture from crossing an interface between two perfectly bonded layers; instead, they limit the depth of penetration into the barrier layers (van Eekelen 1982). Results show that it takes a rather long penetration distance into the higher-stress layer (many times the characteristic thicknesses of the formation layers) for the fracturing pressure to increase to the *in situ* stress value in that layer. For instance, in this particular case $h_0 = 10 \text{ m}$ and $\Delta\sigma = 2 \text{ MPa}$, the fracturing pressure is still lower than the closure stress in the higher-stress layer even after more than 100 m of penetration into it, which is 10 times the half-height of the middle layer. Overall, the comparison indicates an excellent agreement of MVCCT and DEDM results with the analytical solution.

The influence of the mesh resolution on the net fracturing pressure prediction is further investigated, as shown in Fig. 4(a). Four mesh resolutions, $\Delta h = 0.5 \text{ m}$, 0.25 m , 0.125 m , 0.0625 m are adopted in the simulations. The relative errors of MVCCT compared with the analytical solution, along with results of DEDM on a fine mesh resolution ($\Delta h = 0.0625 \text{ m}$), are shown in

Fig. 4(b). The greatest error is observed when the tip is at the interface, which is expected as the next virtual growth of the fracture is into a region (layer) under a very different stress state. However, the error is shown to be significantly mitigated with mesh refinement. Meanwhile, the error is more sensitive to the element size after the fracture penetrates into the stress barrier layer than that before the penetration. In addition, as a comparison, the error of DEDM is consistently smaller than that of MVCCT, supporting our validation approach of using the DEDM with sufficiently fine mesh resolution as a reference for evaluating the accuracy of MVCCT when analytical solutions are not available.

Next, we evaluate the accuracy of MVCCT for various magnitudes of the stress jump. Since the analytical solution indicates that the net fracturing pressure is not affected by the magnitude of stress jump until the fracture tip reaches the barrier, we focus on the results when the fracture tip is at stress interface and has entered the higher-stress layer. Fig. 5(a) and (b) show the net fracturing pressure comparison between MVCCT and the analytical solutions, as well as the corresponding relative error. It can be seen that the error between MVCCT and the analytical solution increases with increasing magnitude of stress jump as a result of the violation of fracture tip region self-similarity condition, which is evident from the non-elliptical fracture geometry in Fig.2 compared with classic 2D elliptical (self-similar) fracture. A greater stress contrast crossing the interface is expected to result in more deviation of fracture tip geometry from self-similarity. Although a substantial error is observed at the interface, the error diminishes rapidly when the tip enters into the second layer. With a fairly large stress contrast $\Delta\sigma = 8$ MPa, the relative error is only about 2% at 0.75 m into the higher-stress layer. These results demonstrate the applicability of MVCCT, even under very large stress contrast.

5.2 Fracturing near a stiffness contrast

According to the theory of LEFM, the SIF diminishes to zero as at the tip of a crack approaching the interface to a stiffer material (Hilton and Sih 1971; Cook and Erdogan 1972). Consequently, it has been argued that a crack would not cross into a stiffer material from a softer layer in an idealized situation (Simonson et al. 1978). This argument, however, contradicts both field observations and laboratory experiments (Nolte and Smith 1981; Warpinski et al. 1982; Smith et al. 1982; Teufel and Clark 1984; Palmer and Sparks 1991; Warpinski et al. 1998; Wright et al. 1999). The reasons for this discrepancy include the applicability of the fracture propagation

criterion $K_I = K_{Ic}$ that is only derived for linearly elastic homogeneous material, the transition zone between layers, and the existence of natural flaws (van Eekelen, 1982).

In this section, two formation layers with differing stiffness are assumed to be perfectly bonded, making other interface properties irrelevant for this problem. We evaluate fracture propagation under two end-member assumptions regarding rock resistance to fracturing. First, the fracture toughness is assumed to be uniform across all layers, reflecting the notion that fracture toughness does not show a clear dependence on rock types (van Eekelen 1982; Thiercelin et al. 1989). Eq. (2) therefore is used to calculate corresponding G_c using the Young's modulus in each formation layer. In the second set of analyses, a uniform critical energy release rate $G_c = 93.75 \text{ J/m}^2$ for all layers is assumed for comparison. Note that the goal of this section is to evaluate the applicability of MVCCT to a fracture that extends a certain distance into a layered rock affected by Young's modulus contrast without imposing a difference in fracture toughness K_{Ic} or critical energy release rate G_c across the layers. The summary of model parameters is listed in Table 2.

Fig. 6 illustrates the fracture configuration in a three-layered system with different moduli used for the following studies. The system is symmetric with a half height of the mid-layer $h_0 = 10 \text{ m}$. The baseline study uses an extremely high contrast on Young's modulus $E_2 = 10E_1 = 100 \text{ GPa}$, while all other parameters are assumed to be the same for all layers. Fig. 7 shows the comparison of energy release rate G under a constant net pressure $\Delta p = 0.4 \text{ MPa}$ as a function of fracture tip location, calculated using MVCCT with different mesh resolutions, against a benchmark solution using DEDM on a fine mesh resolution $\Delta h = 0.0625 \text{ m}$. Fig. 8 (a) and (b) show the net fracturing pressure under the same configuration, assuming uniform G_c and K_{Ic} in all layers, respectively.

Unlike the previous stress contrast scenario in section 4.1 where the net fracturing pressure in the mid-layer is largely unaffected by the state/property of the next layer until the tip arrives at the interface (Fig. 3), in the stiffness contrast scenario, an adjacent layer with higher stiffness starts to elevate the net fracturing pressure in the lower-stiffness layer as the tip approaches the interface. Note that although the fracturing pressure tends to decrease as the fracture becomes longer in a uniform medium, we observe significant, progressive fracturing pressure increase with fracture propagation in this stiffness contrast scenario, as shown in Fig. 8. Theoretically, the SIF tends to

zero as the fracture approaches an interface from a low-modulus layer to a high-modulus layer. It is not surprising that mesh-based numerical methods, including MVCCT and DEDM, deviate significantly from the asymptotic solution near the interface as a result of discretization errors.

It is also interesting to note that the MVCCT yields a significant overprediction of energy release rate, and thus an underprediction of net fracturing pressure, at the interface compared with the benchmark DEDM results. This can be attributed to the failure of the self-similarity assumption of the trailing nodes as the fracture passes the interface. Specifically, as the tip node is on the interface, the opening at the trailing nodes (i.e., fracture opening w_b in Equation 1) is used as an estimate of the potential opening at the location of the tip for the calculation of energy release rate. That is to say, if the trailing nodes are in the softer material, the opening at trailing nodes will be significantly larger than the opening to be experienced at the current tip location as the fracture propagates into a stiffer material. Thus, energy release rate is overcalculated near/at the interface. The relatively large errors are in stark contrast with the accuracy of the VCCT for homogeneous case, which typically yields a much smaller error even with low-resolution meshes. One mitigating factor of this error is that when the modulus contrast becomes very large, it is possible that the induced tensile stress in the high-modulus layer can initiate a new fracture even before the current fracture tip in the low modulus layer reaches the interface, facilitating an abrupt breakthrough (Leguillon et al. 2000; Smith et al. 2001). Once the fracture breaks through the stiffness contrast, the net fracturing pressure decreases with the further extension of fracture height. Overall, results in Fig. 7 and Fig. 8 indicate that MVCCT slightly overestimates the energy release rate before the fracture penetrates into the high-modulus layer and thus predicts a lower net fracturing pressure to break through. In addition, the mesh sensitivity study shows that the relatively coarse mesh resolution $\Delta h = 0.25$ m already provides a prediction with sufficient accuracy for engineering application. However, with a finer mesh ahead of the interface, the net fracturing pressure becomes larger as the asymptote of energy release rate is queried at a smaller distance from the interface. Except for the singularity at the interface, the reasonable match between MVCCT and the DEDM, along with the mesh convergence, indicates the applicability of MVCCT to problems with large stiffness contrast.

Fig. 9 shows a comparison of net fracturing pressure between MVCCT and DEDM when approaching from a low modulus layer to a high modulus layer under two different contrasts $E_2 =$

$10E_1$ and $E_2 = 3E_1$, performed on a fine mesh resolution $\Delta h = 0.0625$ m. Smaller stiffness contrast is shown to elevate the net fracturing pressure to a lesser extent when the fracture is approaching the high modulus layer, and also result in a smaller error compared with DEDM. After the fracture crosses the interface, MVCCT shows an excellent agreement with DEDM for both cases and the error vanishes when the fracture propagates by an element length into the next formation. Under the assumption of uniform toughness K_{Ic} , the influence of stiffness contrast ratio on net fracturing pressure becomes limited after breakthrough, illustrated in Fig. 9(b).

An even smaller modulus contrast $E_2 = E_1/3$ is considered to study the phenomenon when the fracture approaches a low-modulus layer from a high-modulus layer. Fig. 10 show the comparison of energy release rate induced under a constant net pressure $\Delta p = 0.4$ MPa as a function of fracture tip location, calculated using MVCCT with different mesh resolutions, against a benchmark solution using DEDM on a fine mesh resolution $\Delta h = 0.0625$ m. Fig. 11 show the net fracturing pressure under the same configuration, assuming uniform G_c and K_{Ic} in all layers, respectively. An analytical solution for homogeneous material (i.e., no stiffness contrast) is also plotted in red dash line as a reference, showing that G varies linearly with a and net fracturing pressure varies linearly with $1/\sqrt{a}$, where a is fracture half-length. Compared with the previous case as shown in Fig. 9, the stress intensity factor theoretically increases to infinity near the interface and the breakthrough is promoted when the fracture approaches a low-modulus layer from a high-modulus layer. This comparison indicates that the deviation of MVCCT from benchmark DEDM results mainly occurs before reaching the interface, regardless of whether the fracture approaches a higher- or lower-modulus layer. However, once the fracture crosses the interface, the stress intensity factor decreases in the low modulus layer, and further fracture growth becomes much harder, especially under the assumption of uniform toughness K_{Ic} . The same conclusion that the low modulus layers can provide an impediment to fracture height growth is also reached by Gu and Siebrits (2008). In the case when uniform G_c is assumed, i.e., low fracture toughness in the low modulus layer, the fracture height containment effect by low modulus layers will be mitigated. In contrast, if the fracture toughness is assumed to be higher in the low modulus layer and lower in the high modulus layer, the height containment effect due to stiffness contrast will be more pronounced.

Another interesting phenomenon observed under uniform toughness K_{Ic} assumption is that the maximum net fracturing pressure required in the vicinity of the interface is higher than that for

homogeneous stiffness, regardless whether the stiffness in the adjacent layer is higher or lower. Specifically, in Fig. 11(b), the local maximum net fracturing pressure occurs right before crossing the interface for $E_2/E_1 = 3$ but at a certain distance after crossing the interface for $E_2/E_1 = 1/3$, both larger than that for $E_2/E_1 = 1$. In other words, the required pressure to break through a formation with a varying stiffness is larger than its homogeneous counterpart. This may provide some insights on the lamination effect or the composite layering effect (Warpinski et al. 1998) in the field where microseismic observation typically shows a more contained fracture height than that predicted by most existing simulators if no ad-hoc elevated effective toughness is used.

5.3 Fracturing under a complex stress-stiffness profile

As can be seen in previous sections, the net fracturing pressure is continuous crossing stress contrast but singular at the interface of stiffness contrast. Correspondingly, MVCCT prediction generally incurs less error near stress contrast than near stiffness contrast. It is expected that the discretization used in MVCCT or any other numerical methods would generate a relatively larger error near stiffness contrasts due to the singular nature of this problem.

In reality, a stiffness contrast, by itself, has been found to be insufficient to constitute an effective barrier for fracture height containment (Fung et al. 1987). Real rock formation layers with vertically varying moduli are likely to have *in situ* stresses (Teufel and Clark 1984) varying in a corresponding way. Therefore, we evaluate MVCCT under the combined influences of both *in situ* stress and stiffness contrasts, together with varying thicknesses among the layers. The randomly distributed stress and modulus profiles considered are shown in Fig. 12. The stress contrast ranges between 0 and 5 MPa, while the modulus varies between 10 GPa and 40 GPa across adjacent layers. Note that although the two profiles follow the same layering pattern, reflecting the notion that both *in situ* stress and stiffness abruptly change at layer boundaries, the correlation between the two quantities are not necessarily positive to negative. This is because while harder rock may result in greater tectonic stress, the horizontal stress component due to vertical compaction might actually be smaller due to the associated lower Poisson's ratio. The relative importance of these two mechanisms is expected to vary with geologic settings.

Fig. 12 shows the net fracturing pressure as a function of the fracture tip's vertical location relative to the given stress/stiffness profile, calculated using DEDM and MVCCT on a mesh

resolution $\Delta h = 0.0625$ m. The initiation of the hydraulic fracture starts from a low-stress, low-stiffness layer, the location of which is used as the zero-reference depth in the plot. The net fracturing pressure also uses the *in situ* stress of this layer as the reference datum. The results show that the discrepancy between MVCCT and DEDM solution is discernable when the fracture tip is exactly at layer interfaces (i.e., the discrete markers in Fig. 12), similar to the earlier studies. Beyond these interfaces, MVCCT shows an excellent match with the benchmark DEDM solutions, which further confirms the applicability of MVCCT for complex conditions.

6 Conclusions

In this paper, the applicability and accuracy of the modified virtual crack closure technique (MVCCT) for evaluating a hydraulic fracture's potential to break through rock formation interfaces with significant stress and/or stiffness contrasts are assessed against both analytical solutions and a reference numerical method named the direct energy difference method (DEDM). We demonstrate that the underlying self-similarity assumption of MVCCT becomes problematic when the fracture tip is very near or at stress/stiffness interfaces, resulting in moderate errors in predicted fracturing pressure. As reflected by the equilibrium fracture height model, whether a fracture breaks into the next layer is not a binary choice in most scenarios. The truly critical question is the depth of penetration into the next layer. In this regard, MVCCT's relatively large error when the tip is exactly at the layer interface is usually inconsequential as the error in the predicted depth of penetration during fracture propagation is well-bounded.

All simulations in this work are based on a pseudo-static plane-strain model, which should be seen as a vertical cross-section of a vertical hydraulic fracture that predominately grows in the horizontal direction. Although the actual fracture propagation is a complex dynamic process mainly controlled by the competition between horizontal and vertical fracture tip extensions, a simplified pseudo-static model is a very appropriate and effective research framework for the current evaluation. If MVCCT correctly predicts fracture height growth in the plane-strain condition, when implemented into a 3D, LEFM-based fracturing simulator, it will predict the correct growth pattern for vertical and lateral growths simultaneously.

The difficulties in calculating SIF near interfaces of strong stress/stiffness contrasts are not unique to VCCT and its variants. In fact, the underlying formulation of all methods based on

interpreting near-tip nodal displacements assumes a fracture configuration with uniform material and uniform *in situ* stress. Domain integral methods, like the *J*-integral, yield path-dependent results when the fracture tip is on the interface of dissimilar elastic solids and the dissimilarity is along the direction of fracturing (e.g., vertical fracturing in layered formations) (Hutchinson and Suo 1991). Consequentially, the performance of these methods near stress/stiffness interfaces is not expected to be better than that of MVCCT. Therefore, we conclude that MVCCT is a practical method for calculating stress intensity factor, including when the fracture tip is near stress/stiffness interfaces. The error is well-bounded, in terms of the magnitude and the location where the error is significant. We have demonstrated that this is true even when the stress/stiffness contrasts are much larger than typical values in the field. Nevertheless, great precaution should be taken in interpreting simulated results when the fracture tip is near stress/stiffness interfaces. The quantitative analyses of the error in this work provide useful guidance for interpreting fracturing simulation results near stress/stiffness contrasts.

Acknowledgments

This manuscript has been authored by Lawrence Livermore National Security, LLC under Contract No. DE-AC52-07NA27344 with the US. Department of Energy. The United States Government retains, and the publisher, by accepting the article for publication, acknowledges that the United States Government retains a non-exclusive, paid-up, irrevocable, world-wide license to publish or reproduce the published form of this manuscript, or allow others to do so, for United States Government purposes. This document is LLNL report LLNL-JRNL-751676.

References

- Abbas SE, Gordeliy AP, Lecampion B, Chuprakov DA, Prioul R (2014) Limited height growth and reduced opening of hydraulic fractures due to fracture offsets: an XFEM application. In: SPE hydraulic fracturing technology conference, 4–6 Feb, the Woodlands. <https://doi.org/10.2118/168622-MS>
- Adachi JI, Detournay E, Peirce AP (2010) Analysis of the classical pseudo-3D model for hydraulic fracture with equilibrium height growth across stress barriers. *Int J Rock Mech Min* 47(4):625-639. <https://doi.org/10.1016/j.ijrmms.2010.03.008>
- Bazant ZP, Planas J (1998) Fracture and size effect in concrete and other quasibrittle materials. CRC Press, London
- Barree RD (1983) A Practical Numerical Simulator for Three-Dimensional Fracture Propagation in Heterogeneous Media. In: SPE Reservoir Simulation Symposium, 15–18 Nov, San Francisco. <https://doi.org/10.2118/12273-MS>

- Clifton RJ, Wang JJ (1988) Multiple Fluids, Proppant Transport, and Thermal Effects in Three-Dimensional Simulation of Hydraulic Fracturing. In: SPE Annual Technical Conference and Exhibition, 2-5 Oct, Houston. <https://doi.org/10.2118/18198-MS>
- Cooke, ML, Underwood CA (2001) Fracture termination and step-over at bedding interfaces due to frictional slip and interface opening. *J Struct Geol* 23 (2): 223–238. [https://doi.org/10.1016/S0191-8141\(00\)00092-4](https://doi.org/10.1016/S0191-8141(00)00092-4)
- Cook TS, Erdogan F (1972) Stresses in bonded materials with a crack perpendicular to the interface. *Int J Eng Sci* 10(8): 677–697. [http://dx.doi.org/10.1016/0020-7225\(72\)90063-8](http://dx.doi.org/10.1016/0020-7225(72)90063-8)
- Cherepanov GP (1967) The propagation of cracks in a continuous medium. *J Appl Math Mech* 31(3):503–512. [https://doi.org/10.1016/0021-8928\(67\)90034-2](https://doi.org/10.1016/0021-8928(67)90034-2)
- Chen Z, Jeffrey RG, Zhang X (2015) Numerical modeling of three-dimensional t-shaped hydraulic fractures in coal seams using a cohesive zone finite element model. *Hyd Frac J* 2(2):20–37.
- Chuprakov DA, Prioul R (2015) Hydraulic fracture height containment by weak horizontal interfaces. In: SPE hydraulic fracturing technology conference, 3-5 Feb, the Woodlands. <https://doi.org/10.2118/173337-MS>
- Daneshy, AA (1978) Hydraulic Fracture Propagation in Layered Formations. *SPE J* 18(1). <https://doi.org/10.2118/6088-PA>
- Delaney PT, Pollard DD, Ziony JI, McKee EH (1986) Field relations between dikes and joints: emplacement processes and paleostress analysis. *J Geophys Res* 91(B5):4920–4938. <https://doi.org/10.1029/JB091iB05p04920>.
- Fisher MK, Warpinski NR (2012) Hydraulic fracture-height growth: real data. *SPE Prod Oper* 27(1). <https://doi.org/10.2118/145949-PA>
- Fu P, Johnson SM, Settgest RR, Carrigan CR (2012) Generalized displacement correlation method for estimating stress intensity factors. *Eng Fract Mech* 88:90-107. <https://doi.org/10.1016/j.engfracmech.2012.04.010>
- Fung RL, Vijayakumar S, Cormack D (1987) Calculation of vertical fracture containment in layered formations. *SPE Formation Eval* 2(4):518-522. <https://doi.org/10.2118/14707-PA>
- Gu H, Siebrits E (2008) Effect of formation modulus contrast on hydraulic fracture height containment. *SPE Prod Oper* 23(2). <https://doi.org/10.2118/103822-PA>
- Hilton PD, Sih GC (1971) A laminate composite with a crack normal to the interfaces. *Int J Solids Struct* 7(8):913-930. [https://doi.org/10.1016/0020-7683\(71\)90072-2](https://doi.org/10.1016/0020-7683(71)90072-2)
- Hanson ME, Shaffer RJ (1980) Some results from continuum mechanics analyses of the hydraulic fracturing process. *SPE J* 20(2). <https://doi.org/10.2118/7942-PA>
- Hsiao C, El Rabaa AW (1987) Fracture toughness testing of rock cores. In: The 28th U.S. Symposium on Rock Mechanics, 29 Jun–1 Jul, Tucson. ARMA 87-0141
- Huang J, Morris J, Fu P, Settgest RR, Sherman CS, Ryerson FJ (2018) Hydraulic fracture height growth under the combined influence of stress barriers and natural fractures. *SPE J*. <https://doi.org/10.2118/189861-PA>
- Hutchinson JW, Suo Z (1991) Mixed mode cracking in layered materials. *Adv Appl Mech* 29:63-191. [https://doi.org/10.1016/S0065-2156\(08\)70164-9](https://doi.org/10.1016/S0065-2156(08)70164-9)
- Irwin GR. (1957) Analysis of Stresses and Strains near the End of a Crack Traversing a Plate. *J of Appl Mech*, 24:361-364
- Kruger R (2014) Virtual crack closure technique: history, approach, and applications. *Appl Mech*

- Rev 57(2):109–143. <https://doi.org/10.1115/1.1595677>
- Lam KY, Cleary MP (1984) Slippage and re-initiation of (hydraulic) fractures at frictional interfaces. *Int J Numer Anal Met* 8(6):589-604. <https://doi.org/10.1002/nag.1610080607>
- Leski A (2007) Implementation of the virtual crack closure technique in engineering FE calculations. *Finite Elem Anal Des* 43(3):261-268. <https://doi.org/10.1016/j.finel.2006.10.004>
- Leguillon D, Lacroix C, Martin E (2000) Interface debonding ahead of a primary crack. *J Mech Phys Solids* 48(10):2137-2161. [https://doi.org/10.1016/S0022-5096\(99\)00101-5](https://doi.org/10.1016/S0022-5096(99)00101-5)
- Li FZ, Shih CF, Needleman A (1985) A comparison of methods for calculating energy release rates. *Eng Fract Mech* 21(2):405–421. [https://doi.org/10.1016/0013-7944\(85\)90029-3](https://doi.org/10.1016/0013-7944(85)90029-3)
- Li H, Zou Y, Valko PP, Ehlig-Economides C (2016) Hydraulic fracture height predictions in laminated shale formations using finite element discrete element method. In: SPE hydraulic fracturing technology conference, 9-11 Feb, The Woodlands. <https://doi.org/10.2118/179129-MS>
- Liu S, Valko PP (2017) A rigorous hydraulic-fracture equilibrium-height model for multilayer formations. *SPE Prod Oper*. <https://doi.org/10.2118/173335-PA>
- McClure MW, Horne R (2013) *Discrete Fracture Network Modeling of Hydraulic Stimulation: Coupling Flow and Geomechanics*. SpringerBriefs in Earth Sciences.
- Mader D (1989) *Hydraulic proppant fracturing and gravel packing*. 1st Edition. Elsevier Science Ltd.
- Maxwell SC (2011) Hydraulic fracture height growth. *CSEG Recorder*, 36(9):19–22.
- Nolte KG, Smith MG (1981) Interpretation of fracturing pressures. *J Pet Technol* 33(9):1767–1775. <http://dx.doi.org/10.2118/8297-PA>
- Palmer ID, Luiskutty CT (1985) A model of the hydraulic fracturing process for elongated vertical fractures and comparisons of results with other models. In: SPE/DOE Low Permeability Gas Reservoirs Symposium, 19–22 May, Denver. <http://dx.doi.org/10.2118/13864-MS>
- Palmer ID, Sparks DP (1991) Measurement of induced fractures by downhole tv camera in black warrior basin coalbeds. *J Pet Technol* 43(3). <https://doi.org/10.2118/20660-PA>
- Parks DM (1974) A stiffness derivative finite element technique for determination of crack tip stress intensity factors. *Int J Fract* 10:487. <https://doi.org/10.1007/BF00155252>
- Perkins TK, Kern LR (1961) Widths of hydraulic fractures. *J Pet Technol* 13(9):937–949. <https://dx.doi.org/10.2118/89-PA>
- Rice JR (1968) A path independent integral and the approximate analysis of strain concentration by notches and cracks. *J Appl Mech* 35:379–386.
- Raju IS (1987) Calculation of strain-energy release rates with higher order and singular finite elements. *Eng Fract Mech* 28(3):251-274. [https://doi.org/10.1016/0013-7944\(87\)90220-7](https://doi.org/10.1016/0013-7944(87)90220-7)
- Rybicki EF, Kanninen MF (1977) A finite element calculation of stress intensity factors by a modified crack closure integral. *Eng Fract Mech* 9(4):931–938. [https://doi.org/10.1016/0013-7944\(77\)90013-3](https://doi.org/10.1016/0013-7944(77)90013-3)
- Scholz CH (2010) A note on the scaling relations for opening mode fractures in rock. *J Struct Geol* 32:1485-1487. <https://doi.org/10.1016/j.jsg.2010.09.007>
- Settgast R, Fu P, Walsh S, White J, Annavarapu C, Ryerson F (2017) A fully coupled method for massively parallel simulation of hydraulically driven fractures in 3-dimensions. *Int J Numer Anal Method Geomech* 41(5):627–653. <https://doi.org/10.1002/nag.2557>

- Sheibani F, Olson JE (2013) Impact of fracture height on mixed mode fracture propagation: insights from 3d displacement discontinuity modeling. In: 47th U.S. rock mechanics/geomechanics symposium, 23-26 Jun, San Francisco. ARMA 13-596
- Shlyapobersky J, Issa MA, et al. (1998) Scale effects on fracture growth resistance in poroelastic media. In: SPE annual technical conference and exhibition, 27-30 Sep, New Orleans. <https://doi.org/10.2118/48929-MS>
- Shivakumar KN, Tan PW, Newman JC (1988) A virtual crack-closure technique for calculating stress intensity factors for cracked three dimensional bodies. *Int J Fract* 36:43–50
- Simonson ER, Abou-Sayed AS, Clifton RJ (1978) Containment of massive hydraulic fractures. *SPE J* 18(1):27–32. <https://doi.org/10.2118/6089-PA>
- Smith MB, Bale AB, Britt LK, Klein HH, Siebrits E, Dang X (2001) Layered modulus effects on fracture propagation, proppant placement, and fracture modeling. In: SPE annual technical conference and exhibition, 30 Sep–3 Oct, New Orleans. <https://doi.org/10.2118/71654-MS>
- Tracey DM (1971) Finite elements for determination of crack tip elastic stress intensity factors. *Eng Fract Mech* 3(3):255-265. [https://doi.org/10.1016/0013-7944\(71\)90036-1](https://doi.org/10.1016/0013-7944(71)90036-1)
- Thiercelin M, Jeffrey RG, Naceur KB (1989) Influence of Fracture Toughness on the Geometry of Hydraulic Fractures. *SPE Prod Eng* 4(4):435–442. <https://doi.org/10.2118/16431-PA>
- Tada H, Paris P, Irwin G (2000) *The stress analysis of cracks handbook*, third Edition. Wiley-Blackwell. <https://doi.org/10.1115/1.801535>
- Teufel LW, Clark JA (1984) Hydraulic fracture propagation in layered rock: experimental studies of fracture containment. *SPE J* 24(1). <https://doi.org/10.2118/9878-PA>
- Van Eekelen HAM (1982) Hydraulic fracture geometry: fracture containment in layered formations. *SPE J* 22(3). <https://doi.org/10.2118/9261-PA>
- Voegele MD, Abou-Sayed AS, Jones AH (1983) Optimization of stimulation design through the use of in situ stress determination. *J Pet Technol* 35(6):1071–1081. <https://doi.org/10.2118/10308-PA>
- Warpinski NR, Schmidt RA, Northrop DA (1982a) In situ stresses: the predominant influence on hydraulic fracture containment. *J Pet Technol* 34(3):653–664. <https://doi.org/10.2118/8932-PA>
- Warpinski NR, Clark JA, Schmidt RA, Huddle CW (1982b) Laboratory investigation on the effect of in situ stresses on hydraulic fracture containment. *SPE J* 22(3). <https://doi.org/10.2118/9834-PA>
- Warpinski NR, Branagan PT, Peterson RE, Wolhart SL (1998) An interpretation of m-site hydraulic fracture diagnostic results. In: SPE rocky mountain regional/low-permeability reservoirs symposium, 5-8 April, Denver. <https://doi.org/10.2118/39950-MS>
- Weng X, Kresse O, Cohen C, Wu R, Gu H (2011) Modeling of Hydraulic-Fracture-Network Propagation in a Naturally Fractured Formation. *SPE Prod Oper* 26(4). <https://doi.org/10.2118/140253-PA>
- Wright CA, Weijers L, Davis EJ, Mayerhofer M (1999) Understanding hydraulic fracture growth: tricky but not hopeless. In: SPE annual technical conference and exhibition, 3-6 October, Houston. <https://doi.org/10.2118/56724-MS>
- Wu K, Olson JE (2015) Simultaneous Multifracture Treatments: Fully Coupled Fluid Flow and Fracture Mechanics for Horizontal Wells. *SPE J* 20(2). <https://doi.org/10.2118/167626-PA>
- Xie D, Biggers Jr. SB (2006) Progressive crack growth analysis using interface element based on

- the virtual crack closure technique. *Finite Elem Anal Des* 42:977–84.
<https://doi.org/10.1016/j.finel.2006.03.007>
- Zhang X, Jeffrey RG. (2008) Reinitiation and Termination of Fluid-driven Fractures at Frictional Bedding Interfaces. *J of Geophys Res Atmos* 113, B08416.
<https://doi.org/10.1029/2007JB005327>
- Zhang X, Wu B, Jeffrey RG, Connell LD, Zhang G (2017) A pseudo-3d model for hydraulic fracture growth in a layered rock. *Int J Solids Struct* 115–116:208–223.
<https://doi.org/10.1016/j.ijsolstr.2017.03.022>
- Zhou J, Huang H, Deo M (2016) Simulation of hydraulic and natural fracture interaction using a coupled DFN-DEM model. In: 50th US rock mechanics/geomechanics symposium, 26-29 Jun. ARMA 16-739.
- Zhou J, Huang H, McLennan J, Meakin P, Deo M (2017) A dual-lattice discrete element model to understand hydraulic fracturing in a naturally fractured system. *Hydraul Fract J*, 4(2): 66-82.

List of Figures

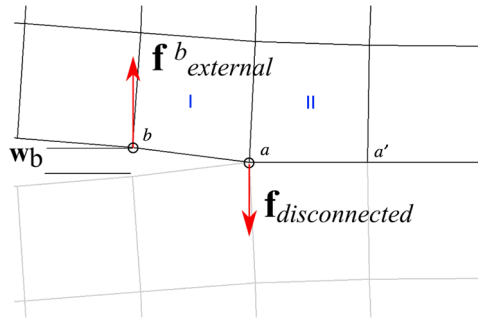


Fig. 1— Mesh configuration for the modified virtual crack closure technique with relevant quantities annotated.

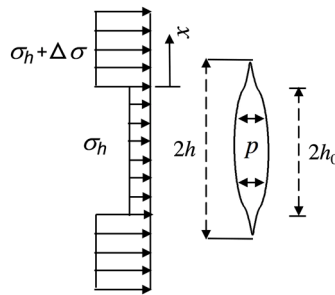


Fig. 2— Configuration of a hydraulic fracture growing into higher-stress formations with uniform fluid pressure inside. Only the upper half of the model is analyzed due to symmetry. A local 1D coordinate system is established with its origin placed at the stress contrast interface. The location of the fracture tip x is the penetration depth into the higher-stress layer.

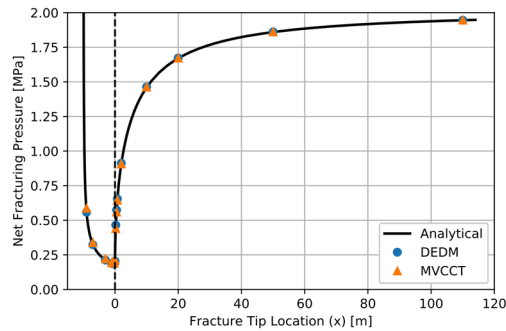


Fig. 3— Comparison of net fracturing pressure of a fracture extending from the midpoint of a 20 m thick, lower-stress layer into an infinite-thickness, higher-stress (by 2 MPa) layer. The dashed line denotes the interface of the stress contrast. The net fracturing pressure is defined as the difference between the fracturing pressure and the minimum horizontal stress in the layer where the fracture initiates.

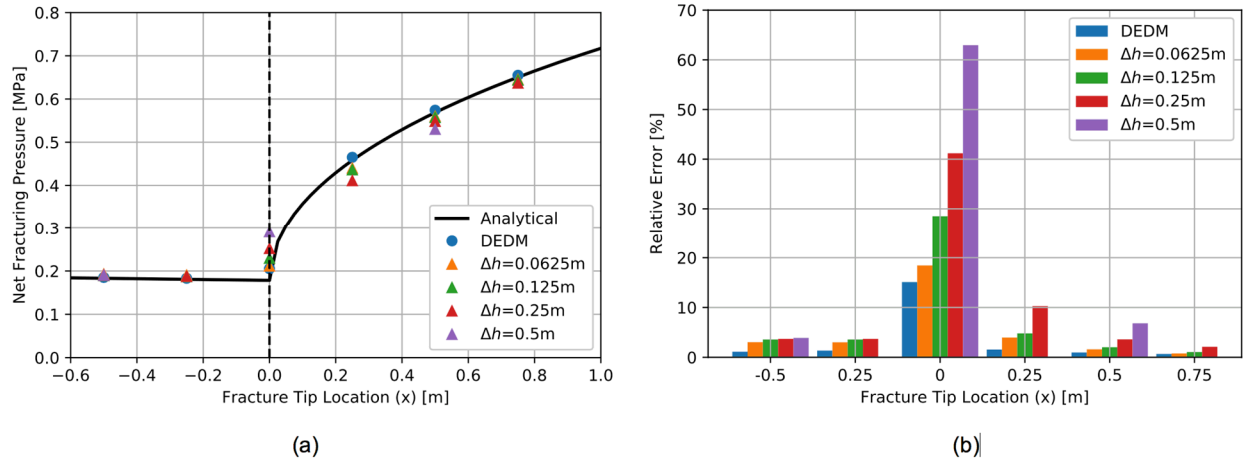


Fig. 4— (a) Comparison of net fracturing pressure near the interface between a fractured, 20 m thick, lower-stress layer and an infinite-thickness, higher-stress (by 2 MPa) layer. MVCCT in four mesh resolutions along with DEDM on a fine mesh resolution $\Delta h = 0.0625$ m is evaluated. (b) The corresponding relative errors of MVCCT and DEDM.

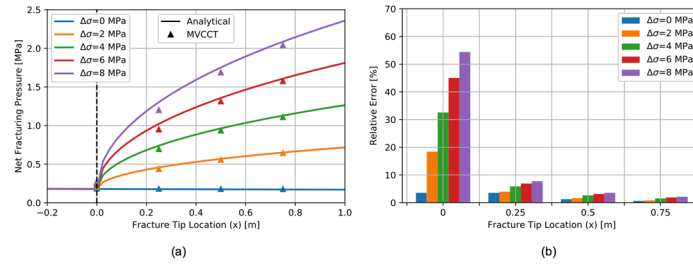


Fig. 5— (a) Comparison of net fracturing pressure near the interface between a fractured, 20 m thick, lower-stress layer and an infinite-thickness, higher-stress layer for various stress difference levels (2 to 8 MPa). MVCCT is evaluated with mesh resolution $\Delta h = 0.0625$ m. (b) The corresponding relative errors of MVCCT.

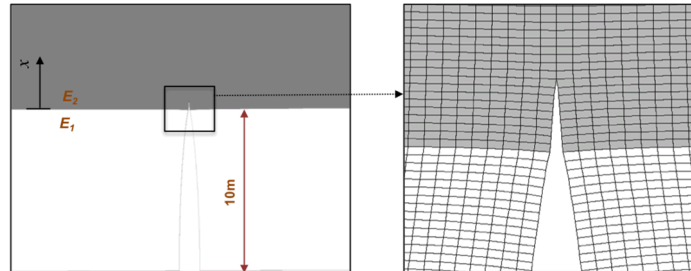


Fig. 6— Fracture configuration near the interface between two materials with distinct Young's moduli, E_1 and E_2 . The symmetry against the lower boundary of the model implies that this is the upper half of a three-layer system similar to that depicted in Fig. 1. The magnified view on the right shows the exaggerated deformation under $E_1 = 10$ GPa and $E_2 = 100$ GPa, with fracture penetration into the upper layer on a mesh resolution $\Delta h = 0.0625$ m along the fracture.

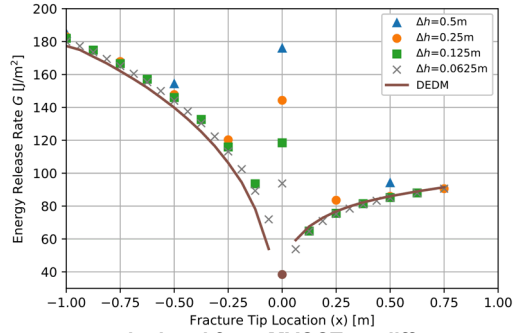


Fig. 7— Comparison of energy release rates calculated from MVCCT on different mesh resolutions against DEDM on the mesh resolution $\Delta h = 0.0625$ m near a large stiffness contrast ($E_2 / E_1 = 10$). A constant net fracturing pressure $\Delta p = 0.4$ MPa is applied.

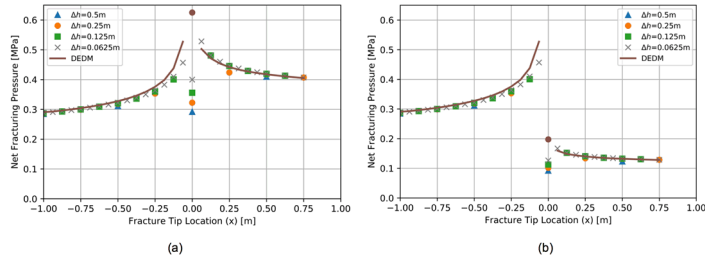


Fig. 8— Comparison of net fracturing pressure calculated from MVCCT on different mesh resolutions against DEDM on the mesh resolution $\Delta h = 0.0625$ m near a large stiffness contrast ($E_2 / E_1 = 10$). Two end-member assumptions regarding the rock resistance to fracturing are considered: (a) uniform G_c and (b) uniform K_c

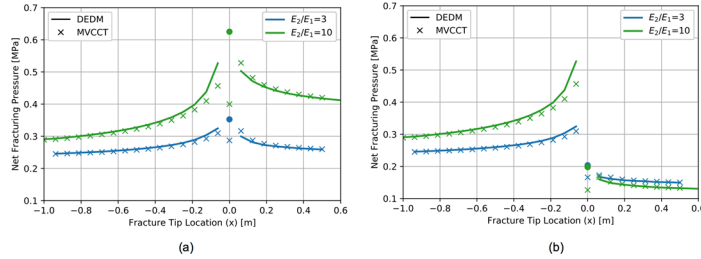


Fig. 9— Comparison of net fracturing pressure when the fracture approaches a high modulus layer from a low modulus layer. Two end-member assumptions regarding the rock resistance to fracturing are considered: (a) uniform G_c and (b) uniform K_c

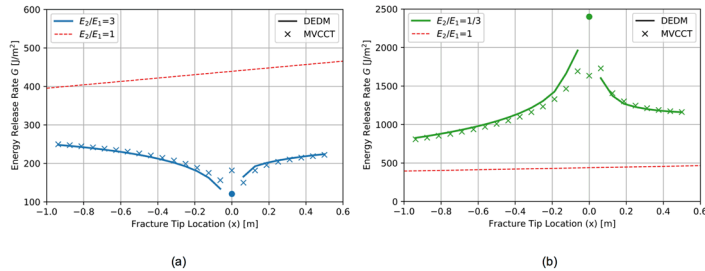


Fig. 10— Comparison of energy release rates calculated from MVCCT on different mesh resolutions against DEDM on the mesh resolution $\Delta h = 0.0625$ m near a stiffness contrast (a) $E_2 / E_1 = 3$ and (b) $E_2 / E_1 = 1/3$. A constant net fracturing pressure $\Delta p = 0.4$ MPa is applied.

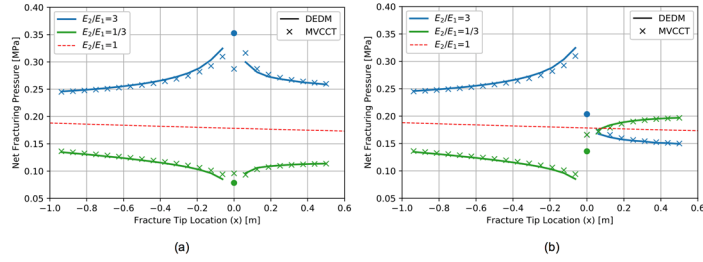


Fig. 11— Comparison of net fracturing pressure on three stiffness contrast levels. Two end-member assumptions regarding the rock resistance to fracturing are considered: (a) uniform G_c and (b) uniform K_{lc}

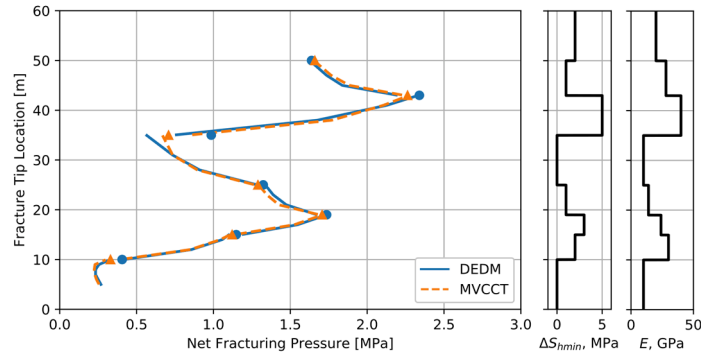


Fig. 12— Variation of net fracturing pressure as a function of the fracture tip location under the combined influence of stress and modulus variations. Fracture initiation depth is used as the reference depth for the vertical axis and the net pressure is relative to the minimum principal stress at this depth. The discrete markers (orange triangles and blue dots) represent calculated net pressure values when the fracture tip is at layer interfaces. Both the stress and stiffness profiles are assumed to be symmetrical against the reference depth.

Table 1—Parameters used in modeling fracturing near a stress contrast homogeneous neous rocks, in comparison with the equilibrium-fracture-height model.

Model parameters	Values
Young's modulus E	10 GPa
Poisson's ratio ν	0.25
Fracture toughness K_{Ic}	1 MPa·m ^{1/2}
Critical energy release rate G_c	93.75 J/m ²
Confining stress of middle layer σ_h	20 MPa
Half-thickness of middle layer h_0	10 m
Stress contrast $\Delta\sigma$	[0, 2, 4, 6, 8] MPa
Mesh resolution Δh	[0.0625, 0.125, 0.25, 0.5] m

Table 2—Parameters used in modeling fracturing near a stiffness contrast under uniform stress.

Model parameters	Values
Young's modulus E_1	10 GPa
Young's modulus E_2	[3.333, 30, 100] GPa
Poisson's ratio $\nu_1 = \nu_2$	0.25
Fracture toughness K_{Ic}	1 MPa·m ^{1/2}
Critical energy release rate G_c	93.75 J/m ²
Mesh resolution Δh	[0.0625, 0.125, 0.25, 0.5] m